Flow in small systems in the EPOS4 approach for high-energy scattering

K. Werner*
SUBATECH, Nantes University–IN2P3/CNRS–IMT Atlantique, Nantes, France

(Received 13 August 2025; accepted 3 December 2025; published 22 January 2026)

EPOS4 is based on a sophisticated (recently significantly improved) parallel-primary-scattering scenario followed by a hydrodynamic expansion, for all collision systems, from small ones such as proton-proton (pp) to large ones such as lead-lead (PbPb). Having already reported on identified particle spectra in recent publications (providing information about radial flow), I discuss here the multiplicity dependence of multiparticle cumulants and flow harmonics, to better understand collectivity in small systems. The model is not particularly tuned for flow results, but it is a "general purpose" approach, trying to accommodate various types of observables with the same model.

DOI: 10.1103/hjb8-pv7p

I. INTRODUCTION

One of the highlights of the past decade in the domain of high-energy scatterings concerns collective phenomena in small systems. It has been shown that high-multiplicity proton-proton (pp) events show very similar collective features as earlier observed in heavy-ion collisions [1], see also the review, Ref. [2]. It is tempting to use the same theoretical tools (hydrodynamic evolution) as in "big systems", and this is what I am going to do.

But here the applicability of viscous hydrodynamics has to be questioned. This issue has been discussed for a long time, see Ref. [3]; for an overview and an extended list of references, see Refs. [2] and [4]. A possible way out is given in terms of hydrodynamics attractors, whose existence has been shown in numerous publications [5–14]. In all cases, the time evolution is given in terms of a single scaling variable $\tilde{\omega}$, with very similar attractor curves, showing a universal behavior at small and large $\tilde{\omega}$, where the latter refers to the late-stage viscous hydro stage [14]. This is encouraging, but it should also be mentioned that these attractor studies employ strong assumptions (boost invariance, conformal symmetry, relaxation-time approximation), so the applicability of viscous hydrodynamics remains an open question.

The present work is complementary to the above theoretical studies. It is often said that viscous hydro "works", but is this really true? I investigate in detail to what extent viscous hydro in the EPOS4 framework is compatible with experimental data, and I try to consider all kinds of observables. Many results have already been published [15–20]. Here I focus on "flow". It should be mentioned that Ref. [19] already studied the question of "flow of charm", but it has not been shown to what extent the "ordinary flow results" (more precisely multiparticle cumulants and flow harmonics) based on light-flavor hadrons can be reproduced in this framework. This paper will fill the gap.

In the EPOS4 approach, one distinguishes "primary interactions" and "secondary interactions". The former refer to parallel partonic scatterings, happening at very high energies instantaneously at $t = 0$, such that any notion of a sequential ordering makes no sense. The theoretical tool is S-matrix theory, using an S-matrix composed of sub-S-matrices representing multiple scattering. The main new development in EPOS4 [15–18] is a way to accommodate simultaneously: (i) rigorous parallel scattering, (ii) energy-momentum sharing, and (iii) validity of the Abramovskii-Gribov-Kancheli (AGK) theorem [21], which assures binary scaling [in nucleus-nucleus (AA) scattering] and factorization [22] [in proton-proton (pp) scattering] for hard processes, by introducing saturation, compatible with recent "low-x-physics" considerations [23–29].

In the following, I will discuss the essential points of the new EPOS4 approach and show why energy-momentum sharing is not only mandatory for a consistent picture, but also allows one to understand a crucial connection between factorization and saturation. See also the "pedagogical presentation" [30]. Let me qualitatively explain it by considering the scattering of two nuclei ($A + B$ with $A = B = 2$) with altogether 3 subscatterings, as sketched in Fig. 1. The two left scatterings represent a double scattering involving the pair of nucleons 2 and 3, whereas the right one is just a single scattering between nucleons 1 and 4. Double scattering (per nucleon-nucleon pair) means energy sharing, so the energy associated with each scattering is small (indicated by small red boxes) compared to a single scattering. However, the saturation scales associated with the double scatterings left are bigger (indicated by big red dots) compared to the single scattering between 1 and 4,

*Contact author: werner@subatech.in2p3.fr

Published by the American Physical Society under the terms of the Creative Commons Attribution 4.0 International license. Further distribution of this work must maintain attribution to the author(s) and the published article's title, journal citation, and DOI. Funded by SCOAP³.

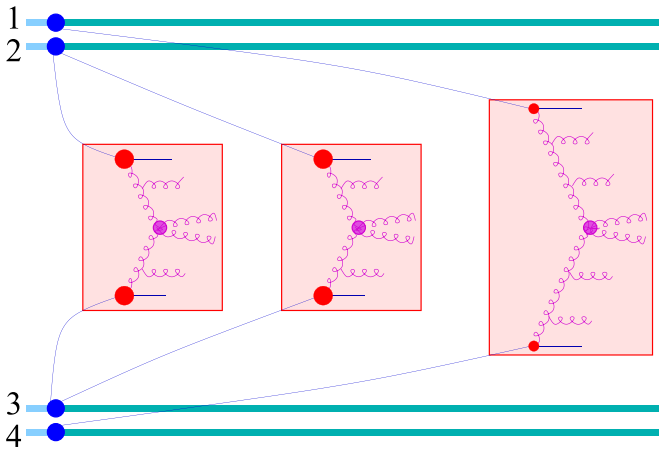


FIG. 1. Sketch of the "compensation" of smaller energies (red box sizes) by larger saturation-scale values (red dots), in a collision of two nuclei with two nucleons each.

and correspondingly, the parton evolution is shorter due to the bigger saturation scale. But *the central part responsible for the hard scattering is identical* in all cases. This last point is the crucial element, which assures that at the end the hard-particle production is independent of the number of scatterings, and therefore the sum of all multiple scattering contributions is (up to a factor) identical to the single-scattering case. And this is what is needed to get factorization (and binary scaling in nuclear scatterings) in such a multiple-scattering formalism.All that means that one can do the same as models based on factorization (defining and using parton distribution functions) to study hard processes (this is needed to prove consistency), but one can do much more, and this is very relevant when it comes to understanding high multiplicity (=multiple-scattering) *pp* events. One of the highlights of the past decade concerns actually collective phenomena in small systems. It has been shown that high-multiplicity *pp* events show very similar collective features as earlier observed in heavy-ion collisions [1].

From the above-mentioned primary interactions, one obtains a more or less important number of prehadrons. A core-corona procedure [31–33] is employed (see Ref. [18] for the currently employed procedure), where the prehadrons, considered at a given proper time τ_0, are separated into "core" and "corona" prehadrons, depending on the energy loss of each prehadron when traversing the "matter" composed of all the others. Corona prehadrons (per definition) can escape, whereas core prehadrons lose all their energy and constitute what is called "core", which acts as an initial condition for a hydrodynamic evolution [33,34]. In the following, in Figs. 2 and 3, I will show the space-time evolution of typical events for small and big systems.

Let me consider a (randomly chosen, but typical) 7 TeV proton-proton scattering event with 6 Pomerons (representing roughly three times the average). In Fig. 2, I plot the energy density in the transverse plane (x, y). I consider two snapshots, namely at the start time of the hydro evolution $\tau_0 = 0.40$ fm/c (upper plot) and a later time τ_1 close to the final freeze-out (lower plot). The initial distribution has an elongated shape (due to the random positions of interacting partons). One can

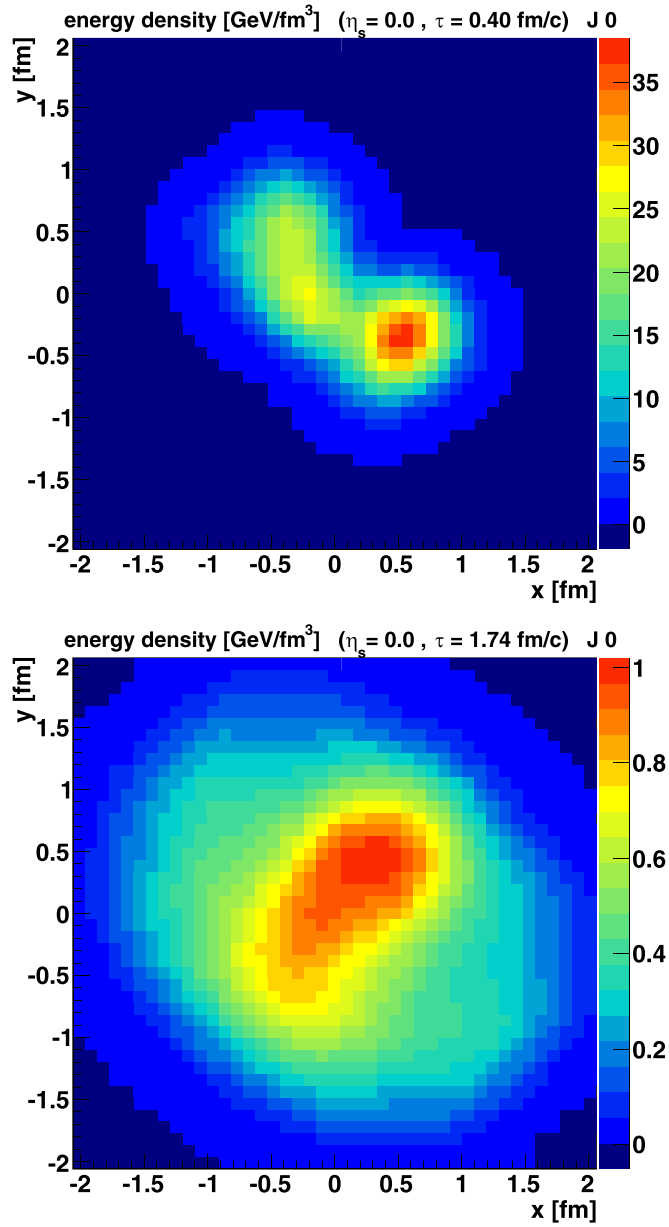


FIG. 2. Energy density of the fluid (core) in the transverse plane (x, y) for proton-proton scattering at 7 TeV involving 6 Pomerons. The upper plot represents the start time τ_0 (of the hydro evolution), and the lower plot a later time τ_1, close to the final freeze-out.

clearly see that the final distribution is also elongated, but perpendicular to the initial one, as expected in a hydrodynamical expansion. In Fig. 3, I plot the energy density in the transverse plane (x, y) for a (randomly chosen, but typical) 5.02 TeV lead-lead scattering event with an impact parameter of 10.4 fm, again considering two snapshots, namely at the start time of the hydro evolution $\tau_0 = 0.40$ fm/c (upper plot) and a later time τ_1 close to final freeze-out (lower plot). The lead-lead plots look very similar to what has been seen before for proton-proton scattering. Also here (for lead-lead), one can see that the final distribution is elongated, perpendicular to the initial one.

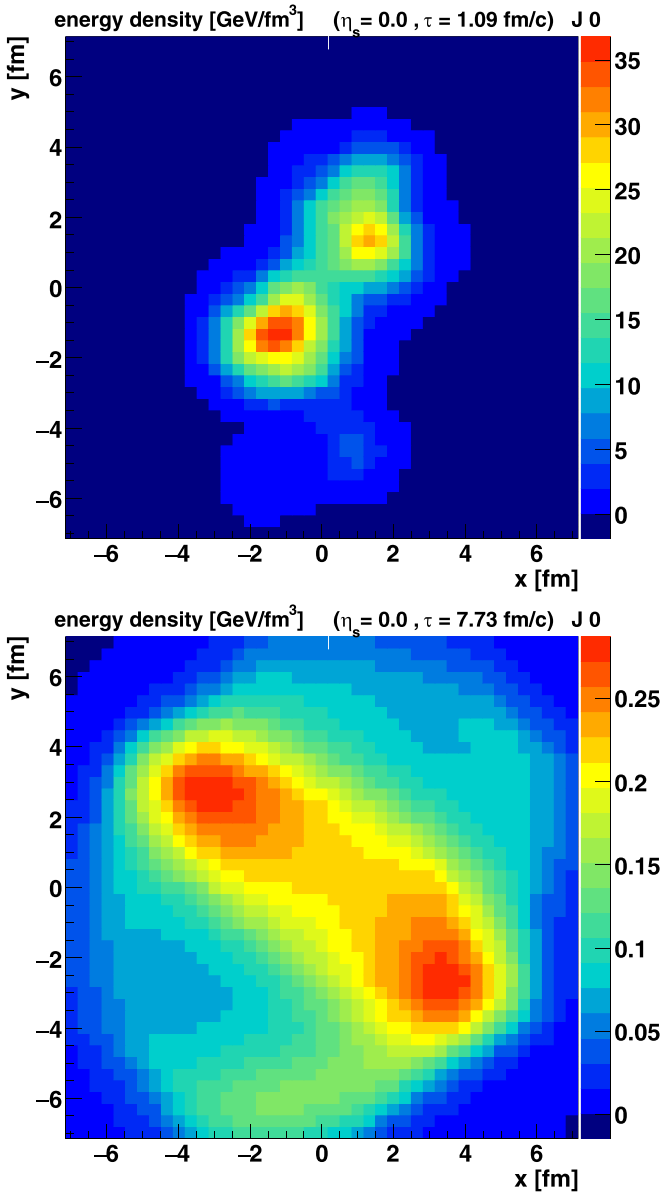


FIG. 3. Energy density of the fluid (core) in the transverse plane (x, y) for a lead-lead scattering at 5.02 TeV with an impact parameter of 10.4 fm. The upper plot represents the start time τ_0 (of the hydro evolution), and the lower plot a later time τ_1, close to final freeze-out.

The Figs. 2 and 3 are just two examples, but looking at more cases, one can see that the space-time evolution of the energy density in proton-proton scattering and lead-lead scattering look very similar. In case of an elongated initial shape, one gets at the end as well an elongated shape, but perpendicular to the initial one, as expected from a hydrodynamic expansion, and which should eventually lead to nonvanishing values for the elliptical flow v_2.

But before coming to the discussion of flow harmonics v_n, based on the momenta of the final particles, one has to mention how to get from a fluid (as shown in the Figs. 2 and 3) to hadrons. The evolution of the core ends whenever the energy density falls below some critical value $\epsilon_{\rm FO}$, which marks the point where the fluid "decays" into hadrons. It is not a switch from fluid to particles, it is a sudden decay, called "hadronization". In EPOS4, as discussed in detail in Ref. [18], a new procedure was developed for computing energy-momentum flow through the "freeze-out (FO) hypersurface" defined by $\epsilon_{\rm FO}$, which allows defining an effective invariant mass, which decays according to microcanonical phase space into hadrons, which are then Lorentz boosted according to the flow velocities computed at the FO hypersurface. Also were developed new and very efficient methods for the microcanonical procedure [18]. Also in the full scheme, including primary and secondary interactions, energy-momentum and flavors are conserved.

II. ELLIPTICAL FLOW IN *pp* COLLISIONS AT 13 TeV, USING THE SYMMETRIC SCENARIO

In Ref. [35], the ATLAS collaboration studies multiparticle cumulants and corresponding Fourier harmonics (or flow harmonics) for small collision systems (pp collisions at $\sqrt{s_{NN}} = 5.02$ TeV) and compares the results with those for Pb + Pb collisions at $\sqrt{s_{NN}} = 2.76$ TeV at low multiplicity. In all cases, cumulants and flow harmonics are presented as a function of the charged-particle multiplicity $N_{\rm ch}$, defined in the same way for the different systems (referred to as $\langle N_{\rm ch}(p_{\rm T} > 0.4)\rangle$in Ref. [35]). Popular procedures to determine flow harmonics are the cumulant method [36,37], based on Refs. [38–40], and the scalar product method [41,42] (see also Appendix A), where the former is employed in Ref. [35]. In addition, a requirement of a pseudorapidity gap $|\Delta\eta| > 2$ may be implemented in calculating the two-particle cumulants, in order to reduce the so-called nonflow effects.

In Fig. 9 of Ref. [35], one compares the multiplicity dependence of the elliptical flow v_2 (with a pseudorapidity gap of 2 units) for different systems, showing a completely different behavior. Whereas for Pb-Pb one observes a strong increase, the pp results are constant. The heavy-ion curve is (at least qualitatively) easy to understand. An important "source" for creating elliptical flow is the initial elliptical shape of the overlap zone, in semiperipheral collisions. Going to very peripheral ion-ion collisions, the overlap zone vanishes, only very peripheral nucleons participate in the scattering, which leads to a decrease of the elliptical flow. A constant elliptical flow in pp is not so easy to understand, so I will investigate this in the following.

There will be many plots with simulations compared to data. In all cases, the simulation results will be presented as "error bands", i.e., two lines of the same color and style, representing $y + \Delta y$ and $y - \Delta y$. Here, y refers to the mean of the plotted variable and Δy to the standard error of the mean.

Let me first discuss results from EPOS4 simulations without hydrodynamical evolution, i.e., only primary scatterings. In Fig. 4, I plot the corresponding elliptical flow $v_2\{2\}$ with a pseudorapidity gap of 2 units, in short $v_2\{2, |\Delta\eta| > 2\}$, as a function of the multiplicity $N_{\rm ch}$, in pp collisions at 13 TeV (blue lines), compared with the data from ATLAS [35] (black points). The theoretical results represent a so-called "nonflow" contribution, because per construction there is no fluid involved, so the correlations have a different origin, like dijet

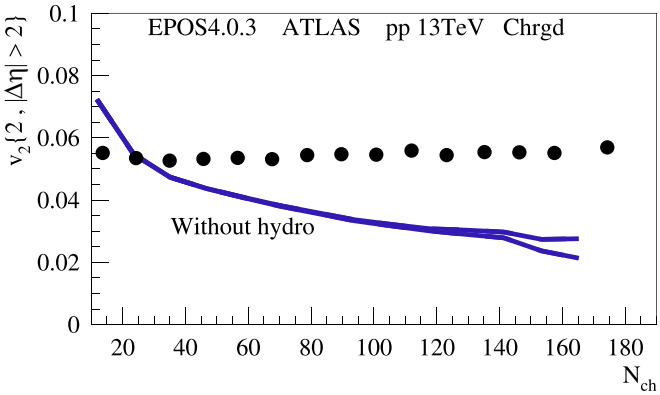


FIG. 4. Elliptical flow $v_2\{2, |\Delta\eta| > 2\}$, shown as a function of the multiplicity N_{ch}, in pp collisions at 13 TeV. Compared are the simulations without hydro (blue lines, representing an error band) with data from ATLAS [35] (black points).

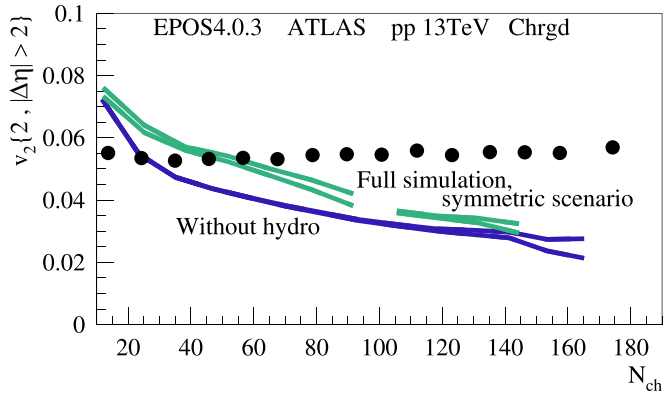


FIG. 5. Same as Fig. 4, but in addition the full simulation, using the symmetric scenario (green broken lines). Again I show error bands.

production. As expected, the curve drops with increasing multiplicity. One can see that despite the application of a rapidity gap of two units, meant to reduce nonflow effects, the latter are significant at low multiplicity.

Let me now consider the full simulation, including core-corona procedure, hydrodynamic evolution of the core, and hadronic cascade. An important issue for creating azimuthal asymmetries is a corresponding asymmetry in the initial matter distribution, where the latter is determined by the positions in the transverse plane of the colliding partons. Traditionally (as realized in EPOS3), the transverse positions $\vec{b}_i$ of the partons i relative to the nucleon center are generated as

$$\vec{b}_i = b_i(\cos\varphi_i, \sin\varphi_i), \tag{1}$$

where the φ_i are random angles in $[0, 2\pi]$ and the b_i are random numbers generated according to some simple law $f(b)$, for $1 \leqslant i \leqslant N$ in case of multiple (N-fold) scattering. Since the laws are perfectly symmetric, one refers to this approach as "symmetric scenario". The only source of asymmetery is the randomness in the event-by-event treatment, but there is no geometric origin as in the case of heavy-ion collisons. For completeness it should be said that there is some geometrical effect due to finite impact parameters, but for the (interesting) multiple-scattering events, the impact parameters are very small.

Before discussing simulation results, one needs to overcome some technical challenges. In Fig. 4, results are presented up to multiplicies of $N_{ch} = 190$. But doing now full simulations, including hydrodynamic evolutions, it becomes impossible to go so far. As shown in Appendix B, one may use the number of Pomerons as a trigger to generate high-multiplicity events. I will therefore do minimum-bias simulations, but show results only up to $N_{ch} = 100$, and then simulate events with more than 12 Pomerons, but show results only beyond $N_{ch} = 100$. This method helps, because the first part of the simulation (to determine the number of Pomerons) is fast. The following results will be shown as "broken lines", with the different pieces corresponding to different triggers.

In Fig. 5, I consider the full simulation, using the "symmetric scenario", and plot the corresponding elliptical flow $v_2\{2, |\Delta\eta| > 2\}$, as a function of the multiplicity (green broken lines). The elliptical flow for the full simulation (including hydro evolution of the core) is bigger than the one without hydro (without core-corona procedure), but the curve is not at all flat like the ATLAS data, but it quickly decreases with multiplicity, well below the data points. It even approaches the (blue) nonflow curve at large multiplicity.

Such a failure is actually expected in the symmetric scenario. As already said, the laws of probability concerning the positions in the transverse plane of the colliding partons are symmetric, and an asymmetry only occurs due to the randomness of the event-by-event generation. But increasing multiplicity is correlated with an increasing number of scatterings, having an increasing number of partons (and eventually strings) involved, which makes the initial matter distribution more and more symmetric. And a hydrodynamical evolution based on symmetric initial matter distributions will not produce any v_2. It is therefore unavoidable, in the multiple-scattering formalism, using this "symmetric scenario", to have v_2 vanishing at large multiplicity. In other words, it is impossible to get a flat curve as seen in the ATLAS data.

III. ELLIPTICAL FLOW IN *pp* COLLISIONS AT 13 TeV, USING THE DIPOLE SCENARIO

Already in EPOS4.0.0, the possibility was introduced to change the laws for generating the tranverse positions of the partons. Instead of Eq. (1), one may use

$$\vec{b}_i = b_i(\cos\varphi_i, \sin\varphi_i) \pm \frac{b_{\text{dipole}}}{2}(\cos\varphi_{\text{dipole}}, \sin\varphi_{\text{dipole}}), \tag{2}$$

where the "dipole angle" φ_{dipole} is chosen randomly in $[0, 2\pi]$, but remains the same in case of multiple scatterings. In other words, the partons are now generated around two centers. I refer to this picture as "dipole scenario". The dipole orientations are random, but it happens that in a proton-proton scattering, i.e., the scattering of two dipoles, the orientations are (anti)parallel, creating an elongated initial matter distribution. Therefore, in addition to randomness as an origin of

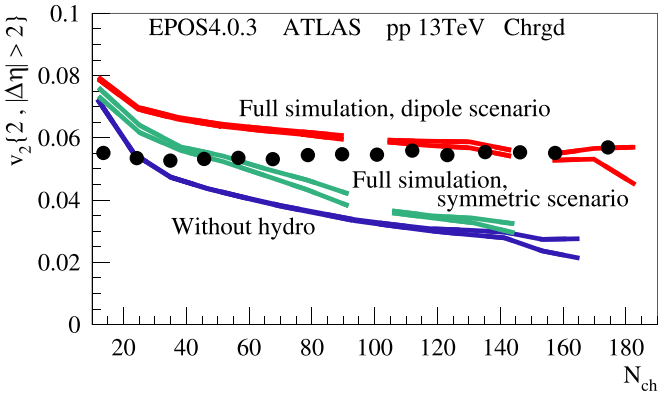


FIG. 6. Same as Fig. 5, but in addition the full simulations, using the dipole scenario (red broken lines). I show error bands for the simulations.

asymmetry, one has here as well a geometric element. This dipole picture was never systematically studied in EPOS4.0.0 publications, the present paper should fill the gap.

In Fig. 6, I consider the full simulation, using the "dipole scenario", and plot the corresponding elliptical flow $v_2\{2, |\Delta\eta| > 2\}$, as a function of the multiplicity (red broken lines). For small N_{ch}, the red curve exceeds the data, it seems that the nonflow is somewhat too big. But beyond a multiplicity of 100, one observes an essentially flat curve, as in the experimental data. Such a behavior is expected, since an increasing number of partons (and strings) does not change the dipole form of the matter distribution. Whereas the flatness of the curve for large multiplicities is a real feature of the approach, its value depends on the parameter b_{dipole}. I take a dipole size b_{dipole} of 1.5 fm.

It is essential that one has here a geometrical feature (the dipole) compared to randomeness as the origin of a possible asymmetry in the symmetric scenario, because the latter leads unavoidably to a continuous decrease of the elliptical flow with increasing multiplicity.

In the above-mentioned ATLAS paper, they present various results concerning the multiplicity dependence of cumulants and flow harmonics. In Fig. 7, I show in addition to the already discussed $v_2\{2, |\Delta\eta| > 2\}$ (upper panel), the cumulants $c_3\{2, |\Delta\eta| > 2\}$ (middle panel), and $c_2\{4\}$ (lower panel). For the definitions, see Appendix A. The data are presented as black dots. Also shown (as red lines) are the EPOS4 results for the full simulation using the dipole scenario. In all cases, for multiplicities beyond 100, the simulations follow the trend of the data. Concerning the hydro evolution, the default value of shear viscosity over entropy density (η/s) of 0.08 is used for all plots. In Fig. 7, in addition, results for $\eta/s = 0.24$ are shown (light green dashed line). At large multiplicity, they are parallel to the curves for $\eta/s = 0.08$, but for $v_2\{2, |\Delta\eta| > 2\}$ it is lower, which would require a larger dipole size to be close to the data.

In order to see the effect due to the dipole feature, I plot in Fig. 8 the corresponding quantities based on full simulations using the symmetric scenario (green lines), and also the ones for simulations without hydro, i.e., the nonflow case (blue dashed lines). The upper panel showns $v_2\{2, |\Delta\eta| > 2\}$, with

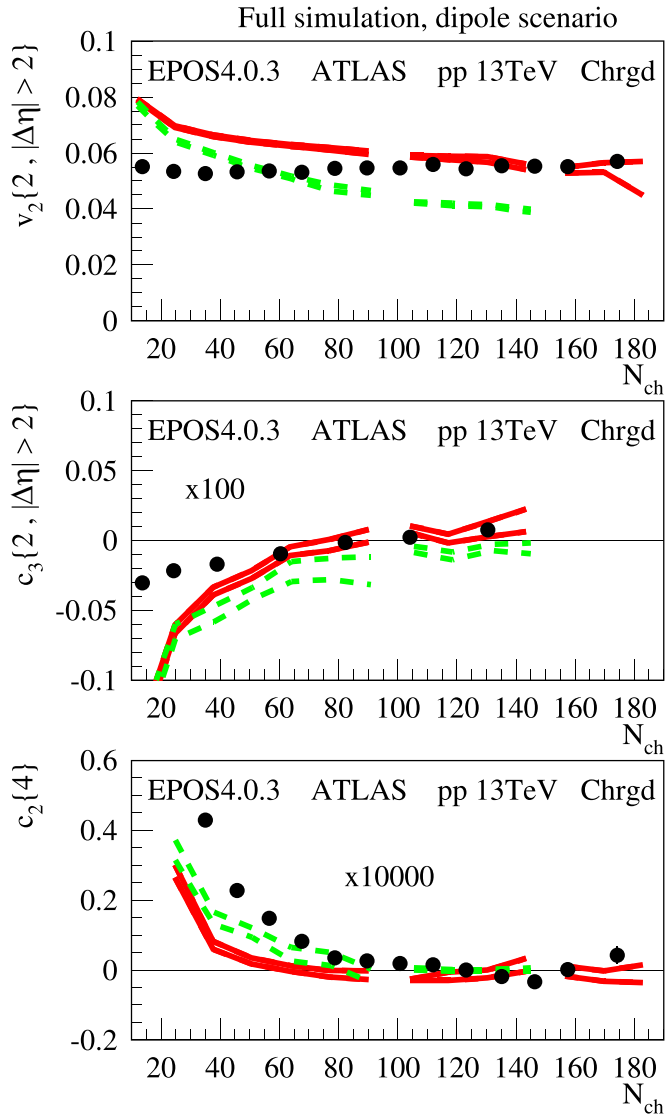


FIG. 7. Flow harmonics and cumulants versus the multiplicity N_{ch} in pp collisions at 13 TeV. One compares the full simulations, using the dipole scenario (red lines), with data from ATLAS [35] (black points). Also shown: results for shear viscosity over entropy density (η/s) of 0.24 (light green dashed). I show error bands for the simulations.

both curves dropping below the data at large multiplicity, as already seen earlier, and here the dipole geometry helps to get close to the data, as shown in Fig. 7.

Concerning the cumulants $c_3\{2, |\Delta\eta| > 2\}$ (middle panel), there is a big negative-nonflow effect (blue dashed lines), getting smaller (but still significant) at larger multiplicities (one cannot go beyond 140 due to limited statistics). The full simulation employing the symmetric scenario (green lines) seems to compensate for the negative nonflow, to give a vanishing cumulant. Comparing this result with $c_3\{2, |\Delta\eta| > 2\}$ for the dipole scenario in Fig. 7, one can see that there is no "dipole effect", which is understandable: The dipole geometry does not help to create triangular initial shapes, the latter are purely random. An important point here: a vanishing cumulant

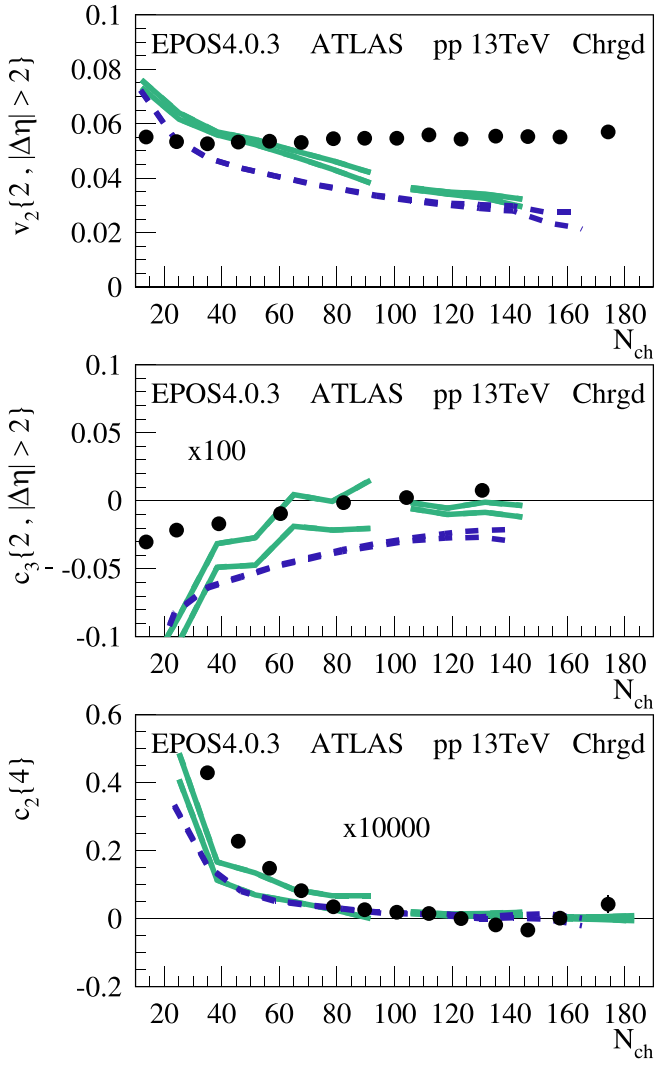


FIG. 8. Cumulants and flow harmonics versus the multiplicity N_{ch}, in pp collisions at 13 TeV. One compares the full simulations, using the symmetric scenario (green lines) and the simulations without hydro (blue dashed lines) with data from ATLAS [35] (black points). I show error bands for the simulations.

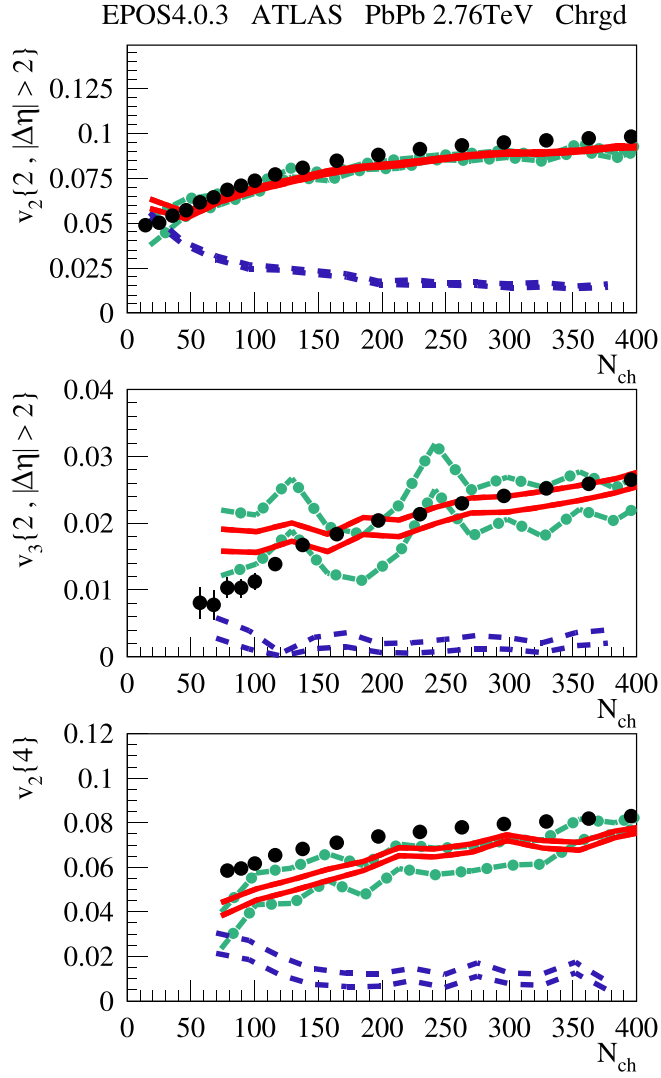


FIG. 9. Different flow harmonics versus the multiplicity N_{ch}, in Pb-Pb collisions at 2.76 GeV. One compares the full simulations using the dipole scenario (red lines), the full simulations using the symmetric scenario (green dot-dashed lines), and the simulations without hydro (blue dashed lines), with data from ATLAS [35] (black points). I show error bands for the simulations.

at intermediate multiplicity is not trivial, it is the result of two effects (nonflow and flow) which compensate each other.

Finally, the four-particle cumulants $c_2\{4\}$ (lower panel) for the simulations without hydro (blue dashed lines) and those of the symmetric scenario (green lines) are roughly zero beyond multiplicities of 80, close to the data. The same can be said concerning the dipole scenario shown in Fig. 7.

IV. HEAVY-ION RESULTS

In Figs. 9, 10, 11, 12, and 13, I will compare experimental data on flow harmonics in Pb-Pb collisions at 2.76 TeV with full EPOS4 simulations, in the dipole scenario, which is the default in EPOS4.0.3, with identical dipole sizes in the case of proton–proton and Pb + Pb collisions. I will also show results for the symmetric scenario and for simulations without hydro. In Ref. [35], not only pp scattering was studied (discussed earlier), but as well low multiplicity Pb + Pb collisions, with the same definition for the multiplicity N_{ch} in both cases. In Fig. 9, I show $v_2\{2,|\Delta\eta|>2\}$ (upper panel), $v_3\{2,|\Delta\eta|>2\}$ (middle panel), and $v_2\{4\}$ (lower panel). For the definitions, see Appendix A. The upper panel shows the elliptical flow (with η gap), i.e., the same quantity as shown in the upper panel of Fig. 8 for pp scattering. Whereas the latter shows a flat behavior, the heavy-ion result shows up as a monotonically increasing curve, with almost no difference between the dipole and the symmetric scenario, both being close to the data.

The fundamental difference between proton-proton and heavy-ion collisions is the fact that increasing multiplicity in the case of proton-proton is due to multiple scatterings involving the same projectile and target nucleon (there is only one),

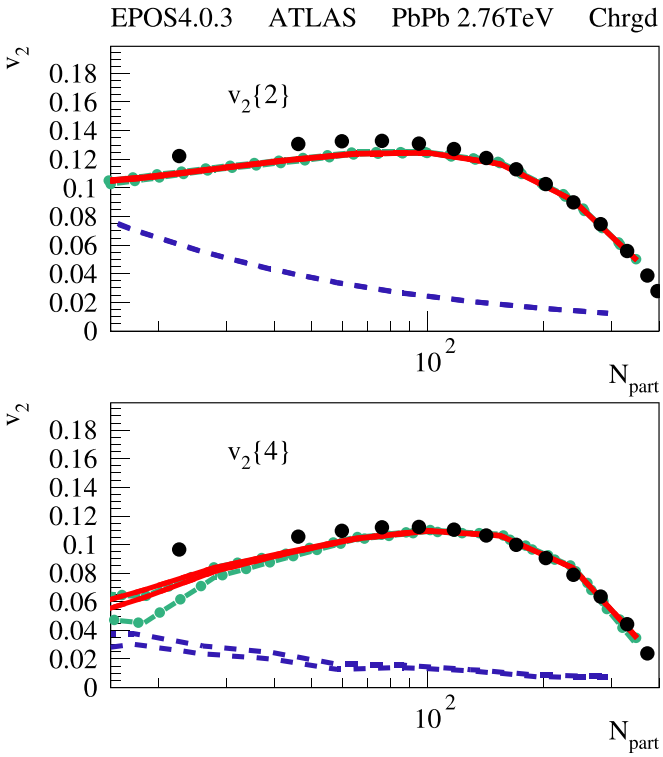


FIG. 10. Flow harmonics $v_2\{2\}$ and $v_2\{4\}$ versus $N_{\rm part}$, in Pb-Pb collisions at 2.76 GeV. One compares the full EPOS4 simulations using the dipole scenario (red lines), the symmetric scenario (green dot-dashed lines), and the simulations without hydro (blue dashed lines), with data from ATLAS [37] (black points). I show error bands for the simulations.

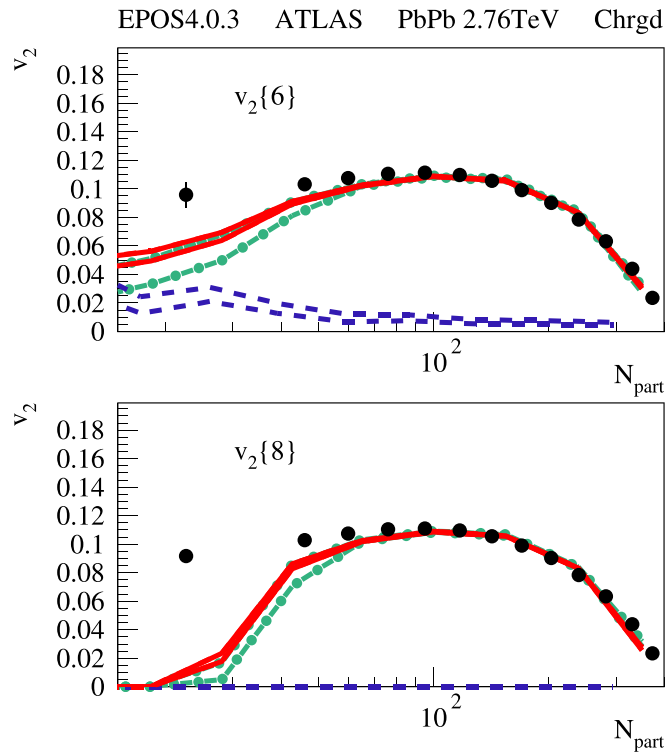


FIG. 11. Flow harmonics $v_2\{6\}$ and $v_2\{8\}$ versus $N_{\rm part}$, in Pb-Pb collisions at 2.76 GeV. One compares the full EPOS4 simulations using the dipole scenario (red lines), the symmetric scenario (green dot-dashed lines), and the simulations without hydro (blue dashed lines), with data from ATLAS [37] (black points). I show error bands for the simulations.

whereas in heavy-ion scattering, the number of participating nucleons increases. Whereas in proton-proton there is a privileged situation where both dipoles are parallel, which counts for all multiple scatterings, in heavy-ion collisions there is a large number of nucleon-nucleon pairs involved, and it is very unlikely that all of them are parallel to each other. As shown by the blue dashed curve, there is also a nonflow effect at small multiplicities, as in proton-proton.

The middle panel of Fig. 9 shows triangular flow $v_3\{2, |\Delta\eta| > 2\}$, with a similar behavior compared to the v_2 result: One can see a monotonically increasing curve, with almost no difference between the dipole and the symmetric scenario, both being close to the data. The absolute size of the triangular flow is smaller than the one for the elliptical flow, because there is no geometric origin for the former.

The elliptical flow (based on four-particle correlations) $v_2\{4\}$ (lower panel) shows a similar behavior to the two-particle result $v_2\{2, |\Delta\eta| > 2\}$, and again there is almost no difference between the dipole and the symmetric scenario, both being close to the data.

In Figs. 10–13, the focus is on flow harmonics based on multiple particle cumulants, as a function of the centrality in terms of the number of participants $N_{\rm part}$, in Pb-Pb collisions at 2.76 GeV. I compare ATLAS data [37] with the full EPOS4 simulations using the dipole scenario (red lines), the full simulations using the symmetric scenario (green dot-dashed lines), and the simulations without hydro (blue dashed lines). The range of $N_{\rm part}$ from 20 to 400 covers all centralities, peripheral ones on the left and central ones on the right.

In Fig. 10, elliptical flow results $v_2\{2\}$ and $v_2\{4\}$ are shown, based on two- and four-particle cumulants. The nonflow effect (blue dashed curves) is smaller in the four-particle case. Again, there is almost no difference between the dipole and the symmetric scenario; both are close to the data, and in both cases the elliptical flow increases up to roughly $N_{\rm part} = 100$, then decreases. The increase in the case of four-particle cumulants is more pronounced.

In Fig. 11, elliptical flow results $v_2\{6\}$ and $v_2\{8\}$ are shown, based on six- and eight-particle cumulants, with results being similar to the two- and four-particle ones.

Also for $v_3\{2\}$, $v_3\{4\}$, $v_4\{2\}$, and $v_4\{4\}$, as shown in Figs. 12 and 13, there is almost no difference between the dipole and the symmetric scenario, and both are close to the data.

V. MORE RESULTS FOR COMPLETENESS

Whereas so far the focus was on the multiplicity (or centrality) dependence of integrated quantities, I will present in the following (in Figs. 14, 15, 16, and 17) more detailed results, i.e., differential quantities versus pseudorapidity or

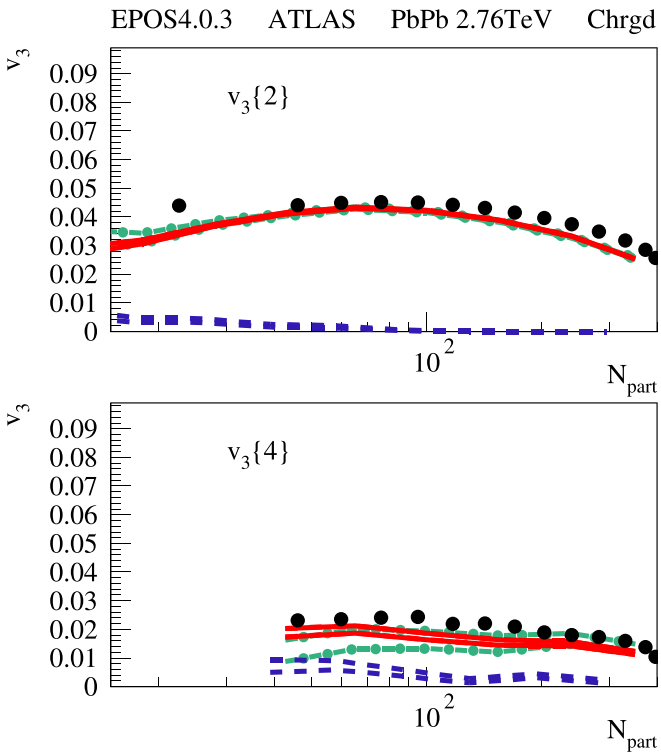


FIG. 12. Flow harmonics $v_3\{2\}$ and $v_3\{4\}$ versus $N_{\rm part}$, in Pb-Pb collisions at 2.76 GeV. One compares the full EPOS4 simulations using the dipole scenario (red lines), the symmetric scenario (green dot-dashed lines), and the simulations without hydro (blue dashed lines), with data from ATLAS [37] (black points). I show error bands for the simulations.

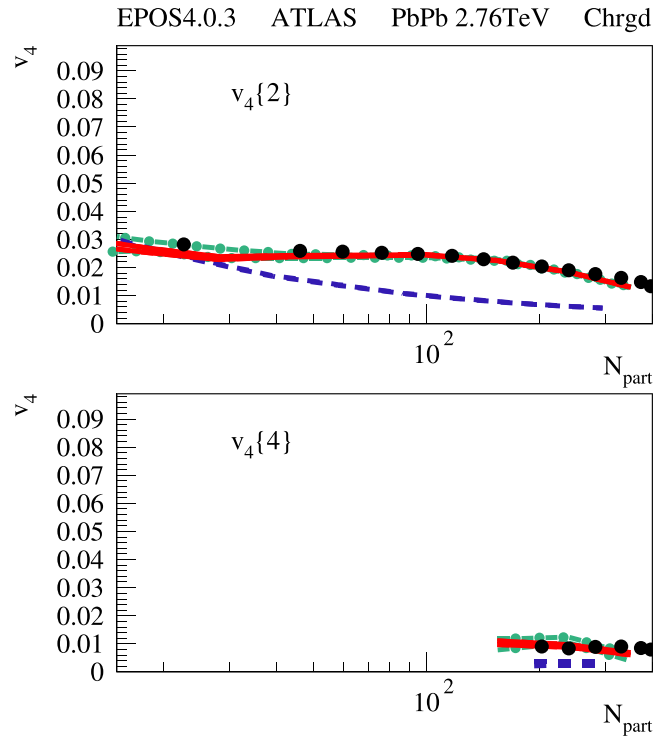


FIG. 13. Flow harmonics $v_4\{2\}$ and $v_4\{4\}$ versus $N_{\rm part}$, in Pb-Pb collisions at 2.76 GeV. One compares the full EPOS4 simulations using the dipole scenario (red lines), the symmetric scenario (green dot-dashed lines), and the simulations without hydro (blue dashed lines), with data from ATLAS [37] (black points). I show error bands for the simulations.

transverse momentum, for different centrality classes, in Pb-Pb collisions at 2.76 GeV. I do not expect new insight, but this is an exercise to check if the approach is consistent.

In Figs. 14 and 15, I show flow harmonics $v_2\{2\}$ and $v_2\{4\}$ versus pseudorapidity η, in Pb-Pb collisions at 2.76 GeV, for different centralities. EPOS4 simulations using the dipole scenario (red lines) are compared with data from ATLAS [37] (black points).

Since I have shown earlier that the Pb-Pb results at 2.76 TeV do not depend much on the scenario, I plot here only results from the full EPOS4 simulations using the dipole scenario, which also represents the default. In general, the simulation results are close to the data, but for semiperipheral collisions beyond 45%, $v_2\{2\}$ is a bit low, whereas the agreement for $v_2\{4\}$ is better. This is compatible with the centrality dependence of integrated flow harmonics shown earlier.

In Figs. 16 and 17, I show flow harmonics $v_2\{2\}$ and $v_2\{4\}$ versus transverse momentum, in Pb-Pb collisions at 2.76 GeV, for different centralities. EPOS4 simulations using the dipole scenario (red lines) are compared with data from ATLAS [37] (black points).

For low and intermediate values of p_t, the simulation results are close to the data again, except for $v_2\{2\}$ in the most peripheral events, where the simulations are slightly below the data.

However, the high p_t region is not well described, simulations are too low, indicating too little energy loss. The latter is treated in EPOS4 in a very simplified fashion in connection with the core/corona procedure, based on a very simple energy-loss method, see Ref. [18].

VI. SUMMARY AND CONCLUSIONS

I discussed in this paper the multiplicity dependence of multiparticle cumulants and flow harmonics, to better understand collectivity in small systems. In the first part, proton-proton collisions at 13 TeV were investigated, where experimental findings show a flat behavior of the elliptical flow $v_2\{2, |\Delta\eta| > 2\}$ as a function of the multiplicity. It has been demonstrated that the full EPOS4 simulation, including a hydrodynamical evolution (and therefore producing flow), cannot have such a flat behavior, if one uses the "symmetric scenario", i.e., distributions of the transverse positions of the partons generated according to a symmetric law, because here an asymmetric behavior is entirely due to the randomness of the event-by-event generation. The randomness disappears with an increasing number of scatterings, associated to an increasing multiplicity. However, if one introduces a geometric component in the form of a distribution of transverse positions around two centers, i.e., the dipole scenario, then one expects and observes a flat v_2 curve as in the data.

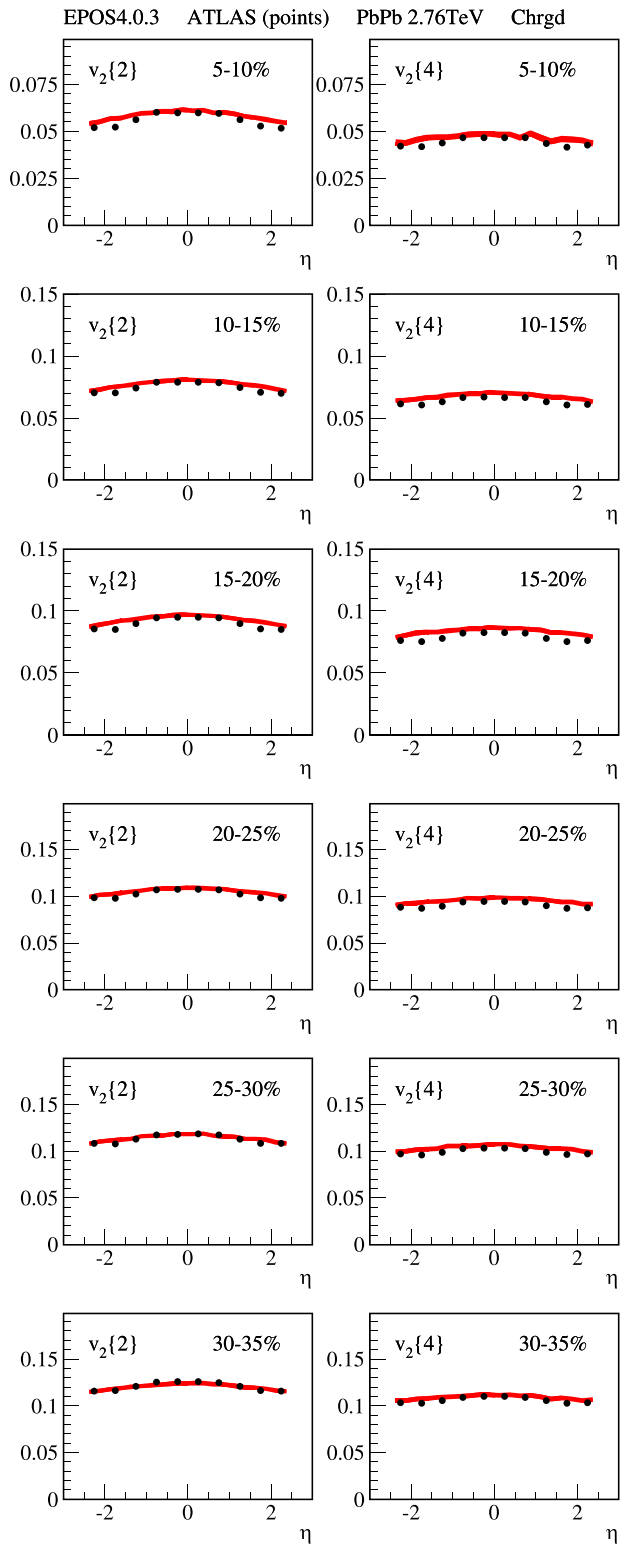


FIG. 14. Results for $v_2\{2\}$ and $v_2\{4\}$ versus pseudorapidity η, in Pb-Pb collisions at 2.76 GeV, for different centralities (below 35%). I compare the EPOS4 simulations using the dipole scenario (red lines) with data from ATLAS [37] (black points). I show error bands for the simulations.

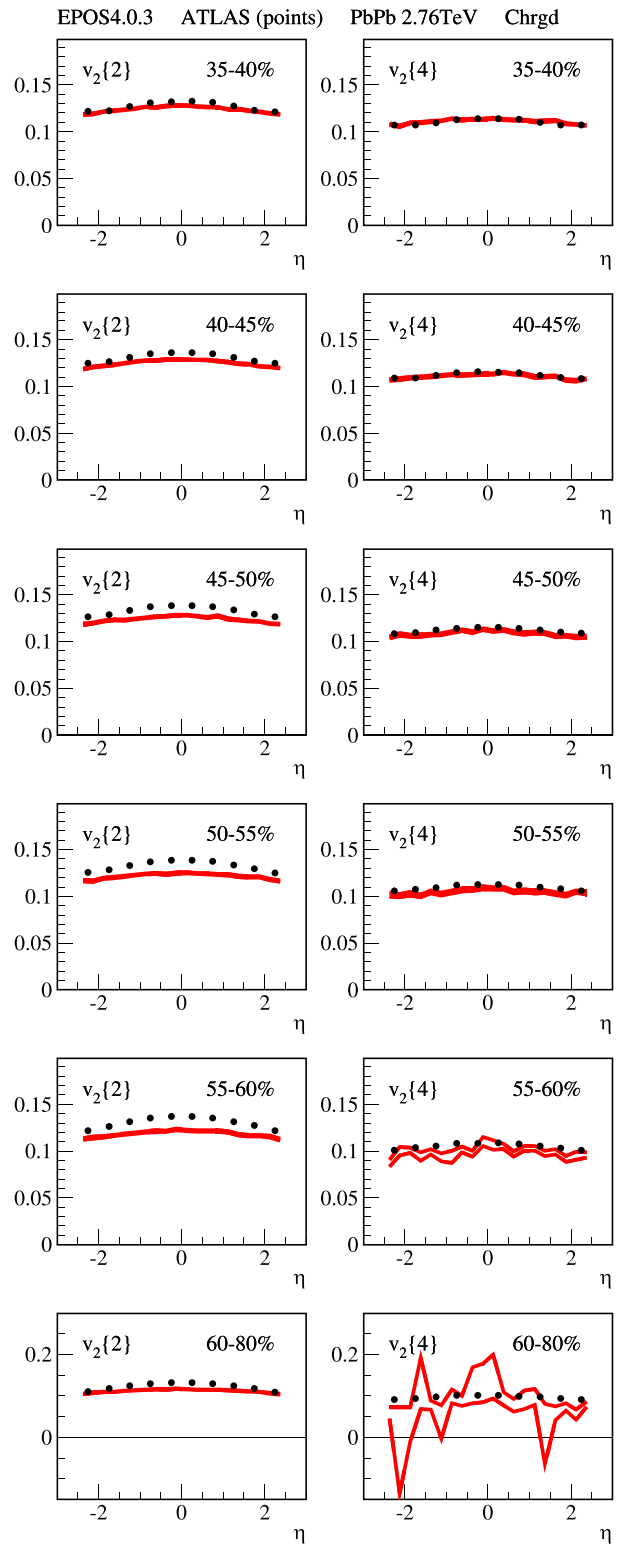


FIG. 15. Results for $v_2\{2\}$ and $v_2\{4\}$ versus pseudorapidity η, in Pb-Pb collisions at 2.76 GeV, for different centralities (above 35%). One compares the EPOS4 simulations using the dipole scenario (red lines) with data from ATLAS [37] (black points). I show error bands for the simulations.

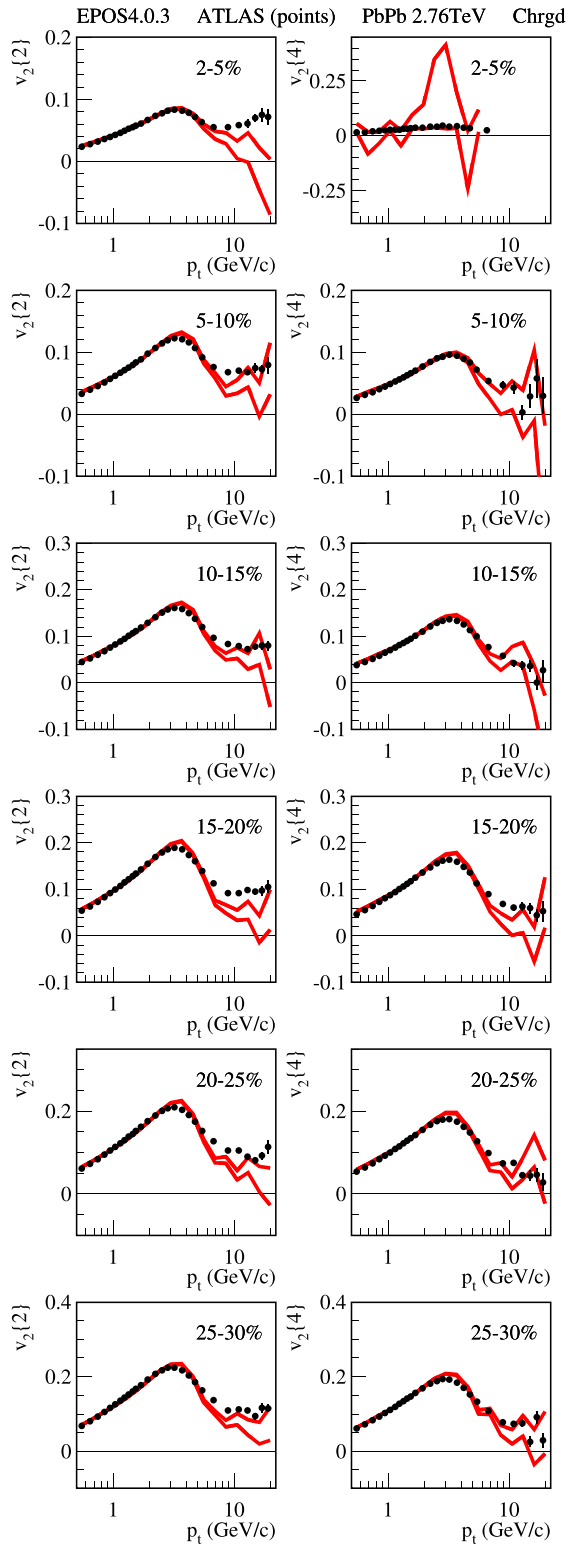


FIG. 16. Results for $v_2\{2\}$ and $v_2\{4\}$ versus transverse momentum, in Pb-Pb collisions at 2.76 GeV, for different centralities (below 30%). One compares the EPOS4 simulations using the dipole scenario (red lines) with data from ATLAS [37] (black points). I show error bands for the simulations.

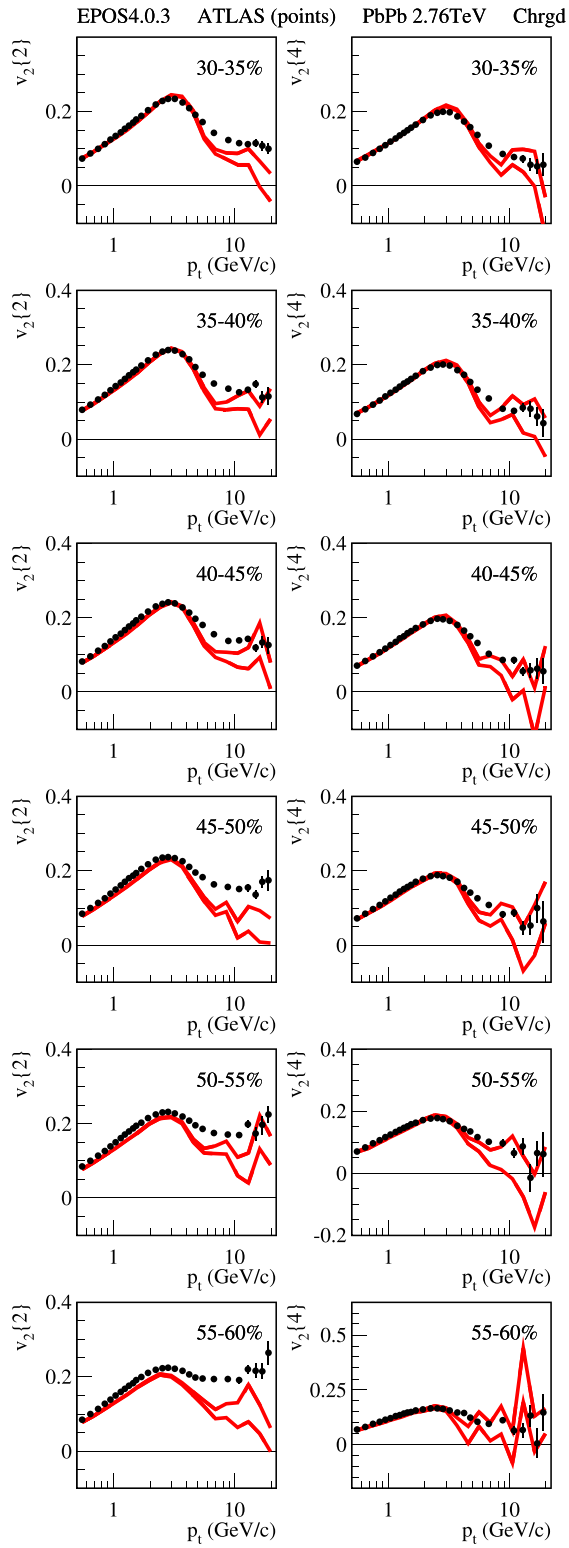


FIG. 17. Results for $v_2\{2\}$ and $v_2\{4\}$ versus transverse momentum, in Pb-Pb collisions at 2.76 GeV, for different centralities (above 30%). One compares the EPOS4 simulations using the dipole scenario (red lines) with data from ATLAS [37] (black points). I show error bands for the simulations.

I then investigated Pb-Pb collisions at 2.76 TeV. It was shown that here the difference between the symmetric scenario and the dipole scenario is small. Actually both scenarios are close to the data. The fundamental difference between proton-proton and heavy-ion scattering is the fact that increasing multiplicity in case of proton-proton is due to multiple scatterings involving the same projectile and target nucleon (there is only one), whereas in heavy-ion scattering, the number of participating nucleons increases. In proton-proton there is a privileged situation where both dipoles are parallel, which is the case for all multiple scatterings, and this provides an asymmetric initial matter distribution. In heavy-ion collisions there is a large number of nucleon-nucleon pairs involved, and it is very unlikely that all of them are parallel to each other, which explains that the dipole geometry is hardly visible.

I have presented results for many different cumulants and flow harmonics in *pp* collisions at 13 TeV and in Pb-Pb collisions at 2.76 TeV, integrated and differential ones, showing that the "dipole scenario", which is the default in EPOS4.0.3, gives in general a good desciption of the data. Exceptions are the very low multiplicity region in proton-proton collisions at 13 TeV, and the high transverse momentum region in Pb-Pb collisions at 2.76 TeV.

The main message of the paper, based on EPOS4 simulations compared to data, is that a dipole form of a high-energy proton is needed to explain flow-harmonics results in small systems, and that such a scenario gives a coherent picture when comparing simulations and a large amount of data on multiparticle cumulants and flow harmonics.

DATA AVAILABILITY

The data that support the findings of this article were generated with a publicly available code [43].

APPENDIX A: COMPUTING FLOW HARMONICS

1. Cumulant method

Following Refs. [36] and [37], based on [38–40], one first discusses the *reference flow*. For given n, the two- and four-particle correlations are defined as

$$\langle 2\rangle = \langle e^{in(\phi_1-\phi_2)}\rangle = \frac{1}{w_2}\sum_{i,j}{}' e^{in(\phi_i-\phi_j)}, \tag{A1}$$

and

$$\langle 4\rangle = \langle e^{in(\phi_1+\phi_2-\phi_3-\phi_4)}\rangle = \frac{1}{w_4}\sum_{i,j,k,l}{}' e^{in(\phi_i+\phi_j-\phi_k-\phi_l)}, \tag{A2}$$

with

$$w_2 = M(M-1), \tag{A3}$$

$$w_4 = M(M-1)(M-2)(M-3), \tag{A4}$$

with M being the multiplicity, counting all particles in a given acceptance, referred to as reference flow particles (RFP), and where $\sum'$ means that all indices in the sum must be taken different. To compute $\langle 2\rangle$, one uses Q_n (called Q vector, although it is actually a complex number and not a vector):

$$Q_n = \sum_{i=1}^{M} e^{in\phi_i}. \tag{A5}$$

One gets $Q_n\bar{Q}_n = M + w_2\langle 2\rangle$, so

$$\langle 2\rangle = \frac{1}{w_2}\{Q_n\bar{Q}_n - M\}. \tag{A6}$$

To compute $\langle 4\rangle$, one uses

$$|Q_n|^4 = Q_nQ_n\bar{Q}_n\bar{Q}_n = \sum_{i,j,k,l} e^{in(\phi_i+\phi_j-\phi_k-\phi_l)}. \tag{A7}$$

One has four distinct cases for the indices i, j, k, l: they are all different (four-particle correlation), three are different, two are different, or they are all the same. One finally gets

$$\langle 4\rangle = \frac{1}{w_4}\{|Q_n|^4 + |Q_{2n}|^2 - 2Re\{Q_{2n}\bar{Q}_n\bar{Q}_n\} - 4(M-2)|Q_n|^2 - 2M(M-3)\}. \tag{A8}$$

Averaging over events gives

$$\langle\langle 2\rangle\rangle = \sum_{\text{events}} w_2\langle 2\rangle \Big/ \sum_{\text{events}} w_2, \tag{A9}$$

and

$$\langle\langle 4\rangle\rangle = \sum_{\text{events}} w_4\langle 4\rangle \Big/ \sum_{\text{events}} w_4. \tag{A10}$$

The *cumulants* are

$$c_n\{2\} = \langle\langle 2\rangle\rangle, \quad c_n\{4\} = \langle\langle 4\rangle\rangle - 2\langle\langle 2\rangle\rangle^2. \tag{A11}$$

This gives estimates for the *harmonics*

$$v_n\{2\} = \sqrt{c_n\{2\}}, \; v_n\{4\} = \sqrt[4]{-c_n\{4\}}. \tag{A12}$$

In the following one discusses the *differential flow*, referring to particles of interest (POI). Per definition, M is the total number of particles labeled as RFP, m_p is the total number of particles labeled as POI, and m_q is the total number of particles labeled both as RFP and POI. One defines

$$\langle 2'\rangle = \langle e^{in(\phi_1-\phi_2)}\rangle = \frac{1}{w_{2'}}\sum_{i=1}^{m_p}\sum_{j=1}^{M}{}' e^{in(\phi_i-\phi_j)}, \tag{A13}$$

and

$$\langle 4'\rangle = \langle e^{in(\phi_1+\phi_2-\phi_3-\phi_4)}\rangle = \frac{1}{w_{4'}}\sum_{i=1}^{m_p}\sum_{j,k,l=1}^{M}{}' e^{in(\phi_i+\phi_j-\phi_k-\phi_l)}, \tag{A14}$$

with

$$w_{2'} = m_pM - m_q, \tag{A15}$$

$$w_{4'} = (m_pM - 3m_q)(M-1)(M-2), \tag{A16}$$

where $w_{4'}$ counts the number of different indices, being the sum of $(m_p - m_q)M(M-1)(M-2)$ and $m_q(M-1)(M-2)(M-3)$. The calculation of $\langle 2'\rangle$ and $\langle 4'\rangle$ will be done based

on Q_n as well as on

$$p_n = \sum_{j=1}^{m_p} e^{in\phi_j}, \quad q_n = \sum_{k=1}^{m_q} e^{in\phi_k}. \tag{A17}$$

One finds

$$\langle 2' \rangle = \frac{1}{w_{2'}} \{ p_n \bar{Q}_n - m_q \}, \tag{A18}$$

and

$$\begin{aligned} \langle 4' \rangle = \frac{1}{w_{4'}} \{ & p_n Q_n \bar{Q}_n \bar{Q}_n - q_{2n} \bar{Q}_n \bar{Q}_n - p_n Q_n \bar{Q}_{2n} - 2M p_n \bar{Q}_n \\ & - 2m_q |Q_n|^2 + 7 q_n \bar{Q}_n - Q_n \bar{q}_n + q_{2n} \bar{Q}_{2n} \\ & + 2 p_n \bar{Q}_n + 2 m_q M - 6 m_q \}. \end{aligned} \tag{A19}$$

Averaging over events gives

$$\langle \langle 2' \rangle \rangle = \sum_{\text{events}} w_{2'} \langle 2' \rangle \Big/ \sum_{\text{events}} w_{2'}, \tag{A20}$$

$$\langle \langle 4' \rangle \rangle = \sum_{\text{events}} w_{4'} \langle 4' \rangle \Big/ \sum_{\text{events}} w_{4'}. \tag{A21}$$

The *cumulants* are

$$c_n'\{2\} = \langle \langle 2' \rangle \rangle, \quad c_n'\{4\} = \langle \langle 4' \rangle \rangle - 2 \langle \langle 2' \rangle \rangle \langle \langle 2 \rangle \rangle. \tag{A22}$$

This gives estimates for the *harmonics*

$$v_n'\{2\} = \frac{c_n'\{2\}}{\sqrt{c_n\{2\}}}, \; v_n'\{4\} = \frac{-c_n'\{4\}}{\sqrt[4]{-c_n\{4\}^3}}. \tag{A23}$$

One may introduce a pseudorapidity gap $\Delta\eta$ for two-particle correlations, by considering for the reference flow two sets of particles in distinct η intervals a and b with a gap $\Delta\eta$ between them. This requires a minor modification of the above formulas. Instead of a multiplicity M, one has two multiplicities M_a and M_b, and for the weight w_2 one has $w_2 = M_a M_b$. Instead of Q_n one has two Q vectors Q_n^a and Q_n^b, and instead of $\{Q_n \bar{Q}_n - M\}$ one takes the real part of $Q_n^a \bar{Q}_n^b$.

2. Scalar product method

Following the Refs. [41,42], one defines three sets of particles, in different pseudorapidity ranges, for example:

A. Particles in the range $-3.7 < \eta < -1.7$ (N_A reference particles),
B. Particles in the range $-1 < \eta < 1$ (N_B labeled particles),
C. Particles in the range $2.8 < \eta < 5.1$ (N_C reference particles).

Then one defines a two-dimensional vector $\vec{Q}_n^S$ for S being any of the sets A or C as

$$\vec{Q}_n^S = \left(\sum_S \cos(n\varphi), \sum_S \sin(n\varphi) \right), \tag{A24}$$

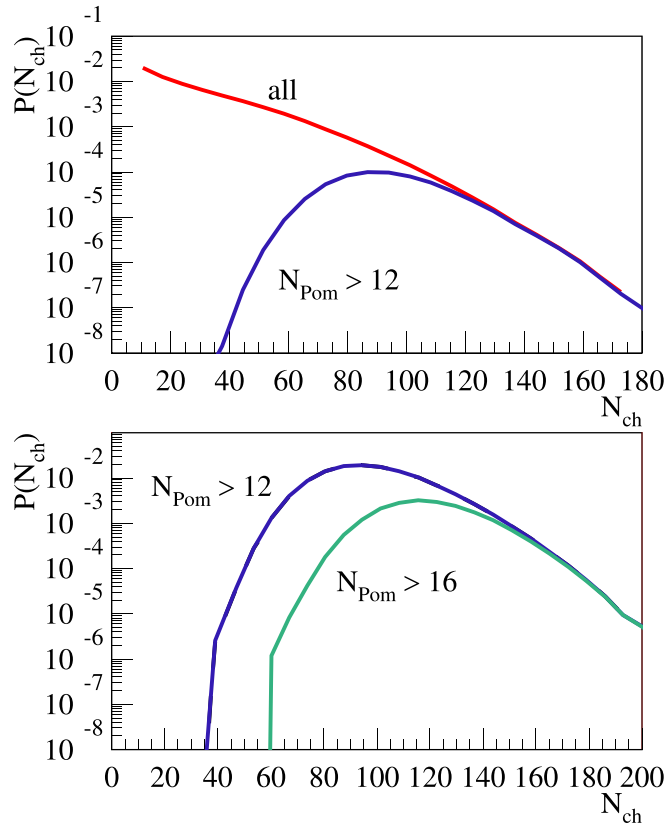


FIG. 18. Multiplicity (N_{ch}) distributions in pp scattering at 13 TeV, where "all" refers to minimum bias results, "$N_{\text{Pom}} > 12$" refers to events with more than 12 Pomerons, and "$N_{\text{Pom}} > 16$" refers to events with more than 16 Pomerons.

and $\vec{q}_n^S = \vec{Q}_n^S / N_S$, so

$$\vec{q}_n^S = (\langle \cos(n\varphi) \rangle_S, \; \langle \sin(n\varphi) \rangle_S). \tag{A25}$$

For each particle in B, one defines

$$\vec{u}_n^B = (\cos(n\varphi), \; \sin(n\varphi)). \tag{A26}$$

The elliptical flow is then

$$v_2 = \sqrt{\frac{\langle \langle \vec{u}_2^B \cdot \vec{q}_2^A \rangle \rangle \langle \langle \vec{u}_2^B \cdot \vec{q}_2^C \rangle \rangle}{\langle \vec{q}_2^A \cdot \vec{q}_2^C \rangle}}.$$

APPENDIX B: HIGH-MULTIPLICITY EVENTS

In Fig. 18, multiplicity distributions in pp scattering at 13 TeV are shown, where "all" refers to minimum bias results, "$N_{\text{Pom}} > 12$" refers to events with more than 12 Pomerons, and "$N_{\text{Pom}} > 16$" refers to events with more than 16 Pomerons. This shows that the number of Pomerons can be used as a trigger to generate high-multiplicity events.

[1] CMS, V. Khachatryan, *et al.*, J. High Energy Phys. 09 (2010) 091.
[2] J. F. Grosse-Oetringhaus and U. A. Wiedemann, arXiv:2407.07484.
[3] R. Baier, A. H. Mueller, D. Schiff, and D. T. Son, Phys. Lett. B **502**, 51 (2001).
[4] V. E. Ambrus, S. Schlichting, and C. Werthmann, Phys. Rev. Lett. **130**, 152301 (2023).

[5] M. P. Heller, R. A. Janik, and P. Witaszczyk, Phys. Rev. Lett. **108**, 201602 (2012).
[6] M. P. Heller and M. Spalinski, Phys. Rev. Lett. **115**, 072501 (2015).
[7] L. Keegan, A. Kurkela, P. Romatschke, W. van der Schee, and Y. Zhu, J. High Energy Phys. 04 (2016) 031.
[8] L. Keegan, A. Kurkela, A. Mazeliauskas, and D. Teaney, J. High Energy Phys. 08 (2016) 171.
[9] M. P. Heller, A. Kurkela, M. Spaliński, and V. Svensson, Phys. Rev. D **97**, 091503 (2018).
[10] P. Romatschke, Phys. Rev. Lett. **120**, 012301 (2018).
[11] M. Strickland, J. Noronha, and G. Denicol, Phys. Rev. D **97**, 036020 (2018).
[12] A. Kurkela, A. Mazeliauskas, J.-F. Paquet, S. Schlichting, and D. Teaney, Phys. Rev. C **99**, 034910 (2019).
[13] M. Strickland, J. High Energy Phys. 12 (2018) 128.
[14] G. Giacalone, A. Mazeliauskas, and S. Schlichting, Phys. Rev. Lett. **123**, 262301 (2019).
[15] K. Werner, Phys. Rev. C **108**, 064903 (2023).
[16] K. Werner and B. Guiot, Phys. Rev. C **108**, 034904 (2023).
[17] K. Werner, Phys. Rev. C **109**, 034918 (2024).
[18] K. Werner, Phys. Rev. C **109**, 014910 (2024), 2306.10277.
[19] J. Zhao, J. Aichelin, P. B. Gossiaux, and K. Werner, Phys. Rev. D **109**, 054011 (2024).
[20] J. Zhao, J. Aichelin, P. B. Gossiaux, V. Ozvenchuk, and K. Werner, Phys. Rev. C **110**, 024909 (2024).
[21] V. A. Abramovskii, V. N. Gribov, and O. V. Kancheli, Yad. Fiz. **18**, 595 (1973).
[22] J. Collins, D. Soper, and G. Sterman, in *Perturbative Quantum Chromodynamics*, edited by A. H. Mueller, World Scientific, Singapore (1989).
[23] L. V. Gribov, E. M. Levin, and M. G. Ryskin, Phys. Rep. **100**, 1 (1983).
[24] L. D. McLerran and R. Venugopalan, Phys. Rev. D **49**, 3352 (1994).
[25] A. Kovner, L. McLerran, and H. Weigert, Phys. Rev. D **52**, 3809 (1995).
[26] Y. V. Kovchegov, Phys. Rev. D **54**, 5463 (1996).
[27] J. Jalilian-Marian, A. Kovner, L. McLerran, and H. Weigert, Phys. Rev. D **55**, 5414 (1997).
[28] J. Jalilian-Marian, A. Kovner, A. Leonidov, and H. Weigert, Nucl. Phys. B **504**, 415 (1997).
[29] J. Jalilian-Marian, A. Kovner, A. Leonidov, and H. Weigert, Phys. Rev. D **59**, 034007 (1999).
[30] K. Werner, arXiv:2410.09955.
[31] K. Werner, Phys. Rev. Lett. **98**, 152301 (2007).
[32] K. Werner, I. Karpenko, T. Pierog, M. Bleicher, and K. Mikhailov, Phys. Rev. C **82**, 044904 (2010).
[33] K. Werner, B. Guiot, I. Karpenko, and T. Pierog, Phys. Rev. C **89**, 064903 (2014).
[34] I. Karpenko, P. Huovinen, and M. Bleicher, Comput. Phys. Commun. **185**, 3016 (2014).
[35] ATLAS, M. Aaboud, *et al.*, Eur. Phys. J. C **77**, 428 (2017), 1705.04176.
[36] A. Bilandzic, R. Snellings, and S. Voloshin, Phys. Rev. C **83**, 044913 (2011).
[37] ATLAS, G. Aad, *et al.*, Eur. Phys. J. C **74**, 3157 (2014).
[38] N. Borghini, P. M. Dinh, and J.-Y. Ollitrault, Phys. Rev. C **63**, 054906 (2001).
[39] N. Borghini, P. M. Dinh, and J.-Y. Ollitrault, Phys. Rev. C **64**, 054901 (2001).
[40] N. Borghini, P. M. Dinh, and J.-Y. Ollitrault, Flow analysis from cumulants: A practical guide, in *International Workshop on the Physics of the Quark Gluon Plasma*, (2001).
[41] STAR, C. Adler, *et al.*, Phys. Rev. C **66**, 034904 (2002).
[42] ALICE, B. B. Abelev, *et al.*, J. High Energy Phys. 06 (2015) 190.
[43] https://klaus.pages.in2p3.fr/epos4/.